Journal of Fluids and Structures (2001) **15,** 929–940
doi:10.1006/jfls.2001.0391, available online at http://www.idealibrary.com on IDEAL®

HYDRODYNAMIC DAMPING OF THE VERTICAL MOTION OF A HORIZONTAL CYLINDER BENEATH WAVES AT LARGE SCALE

J. R. Chaplin and C. H. Retzler

Department of Civil & Environmental Engineering, University of Southampton Highfield, Southampton SO17 1BJ, U.K.

(Received 10 October 2000, and in final form 8 March 2001)

Large-scale laboratory measurements are presented of the hydrodynamic damping of the vertical oscillations of a circular cylinder beneath waves, where the wave crests are parallel to the cylinder axis. In two series of tests, the Stokes parameter β was 647 000 and 997 000, and the Keulegan Carpenter number of the cylinder motion was in the range 0·01–0·1. Observations of the decaying motion of the cylinder, and of steady-state oscillations generated by continuous force excitation, were in reasonable agreement with the vector form of the relative velocity Morison equation with constant coefficients. In some conditions, the motion of the cylinder became phase locked to the wave-induced flow, at an integer frequency ratio.

1. INTRODUCTION

This paper is concerned with the hydrodynamic damping of a horizontal circular cylinder oscillating vertically with small amplitudes beneath waves, whose crests are parallel to the cylinder axis. The relative ambient velocity is the combination of the effect of the rectilinear motion of the cylinder, and the orbital flow due to the waves at a lowest frequency. Since the scale of the waves is much larger than that of the body, the flow is kinematically similar to the case of a cylinder undergoing a complex two-dimensional motion in a fluid initially at rest. Early experiments of this type were carried out by Maull & Milliner (1979) on a cylinder forced to oscillate with a motion having three harmonic components. They observed a proliferation of higher harmonics in the drag, and components at frequencies half-way between the harmonics, and at other unrelated frequencies, in the lift. In another series of experiments at about the same time, Maull & Norman (1979) addressed another complicated aspect of the same problem, that of loading on a stationary cylinder beneath waves with its axis parallel to the wave crests. A practical application of this work—unforeseen 20 years ago—is the problem of predicting the hydrodynamic damping on a pontoon of a tension leg platform (TLP) which is undergoing high-frequency ringing and springing oscillations in waves. This is the focus of the present paper.

Key numbers in this problem include the Stokes parameter $\beta = d^2f/\nu$ (where d is the diameter of the cylinder, f the frequency of oscillation, and ν the kinematic viscosity of water), a reduced velocity $U_r = U/fd$ (where U is the velocity of the ambient flow), and a frequency ratio f/f_w (where f_w is the wave frequency). The amplitude a of the oscillation of the cylinder can be expressed in terms of the Keulegan Carpenter number $K = 2\pi a/d$. Representative values for the case of a TLP are $\beta = 3 \times 10^7$, $U_r = 0{\cdot}3$, $f/f_w = 5$, and the springing and ringing oscillations result in Keulegan Carpenter numbers of the order of 0·01.

0889–9746/01/070929 + 12 $35.00/0

A theoretical starting point is provided by Stokes' (1851) theory, later extended by Wang (1968), for the case of a cylinder undergoing harmonic oscillation in a direction normal to its axis with a small amplitude in a fluid otherwise at rest. This theory is based on the assumption of two-dimensional laminar flow, and by using the approximation $\cos\theta|\cos\theta| \approx (8|3\pi)\cos\theta$, the result can be expressed in terms of a drag coefficient as

$$C_d = \frac{3\pi^3}{2K}\left[(\pi\beta)^{-1/2} + (\pi\beta)^{-1} - \frac{1}{4}(\pi\beta)^{-3/2} + \cdots\right], \tag{1}$$

where the instantaneous force acting on the cylinder per unit length is $C_d[\frac{1}{2}\rho V|V|d]$, and V is its velocity. At large β, equation (1) is closely approximated by

$$C_d = \frac{26{\cdot}24}{\sqrt{\beta}K}. \tag{2}$$

Little is known about the effect of an ambient flow on these results. An analytical solution by Yan (2000) for the case of a steady current predicts only very small changes in the forces.

Achieving the conditions mentioned above in the laboratory presents severe practical problems, and values of β of around 10^6 have only very recently been obtained. A review of the published experimental determinations of C_d in this context is given in Chaplin (2000) for cases in which the amplitude of the motion is less than that which corresponds to the onset of instability—theoretically (Hall 1984) at a critical Keulegan Carpenter number given by

$$K_{\mathrm{cr}} = \frac{5{\cdot}78}{\beta^{1/4}}\left(1 + \frac{0{\cdot}21}{\beta^{1/4}} + \cdots\right). \tag{3}$$

New measurements presented in the same paper for $\beta = 650\,000$ and $1\,250\,000$ were consistent with a level of damping in still water almost exactly twice that predicted by the Stokes/Wang theory (in agreement with earlier results at lower β). The reason for this is not known. In the presence of a slowly varying horizontal current produced by placing the cylinder at the node of very long standing waves, the damping of vertical oscillations was found to increase with the incident reduced velocity at a rate that seemed to depend on the Reynolds number $U_r\beta$.

In the present paper, we report on an extension of the same series of experiments, in which measurements were made of the hydrodynamic damping experienced by the horizontal cylinder constrained to move vertically, in the presence of regular progressive waves, as shown in Figure 1. Attention is focused initially on the way in which the drag coefficient introduced above is influenced by the ambient flow. This approach is referred to as one of "independent flow fields", in which the loading is notionally separated into two components with distinct drag coefficients associated with the high-frequency motion of the cylinder V, and the low-frequency ambient flow U. An alternative procedure (not necessarily any more satisfactory in physical terms) is to use relative velocities in the vector form of Morison's equation, by which the instantaneous vertical force per unit length on the cylinder is

$$F_z(t) = C_{dr}\frac{1}{2}\rho d(U_z - V)\sqrt{U_x^2 + (U_z - V)^2} + C_m\rho\frac{\pi d^2}{4}\dot{U}_z - (C_m - 1)\rho\frac{\pi d^2}{4}\dot{V}, \tag{4}$$

where U_x and U_z are the horizontal and vertical components of the ambient flow, respectively. At very small amplitudes of motion, the single drag coefficient C_{dr} may be expected to approach that which is appropriate for a stationary cylinder in the same ambient flow. For the case of cylinder oscillations of much larger amplitudes, the relative merits of the independent flow fields and Morison's approaches are discussed by Demirbilek *et al.* (1987).

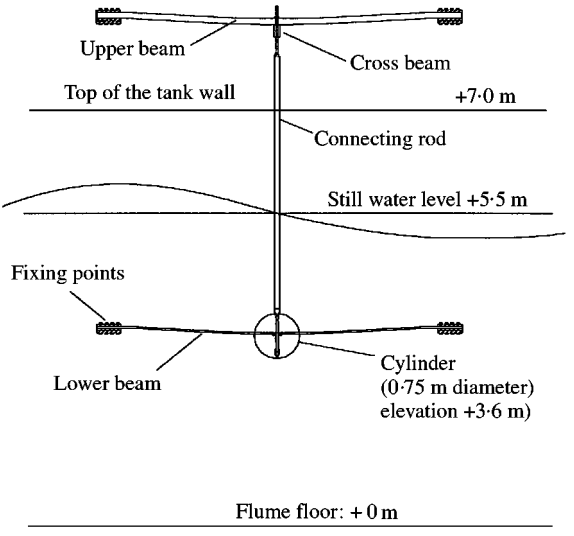

Figure 1. A sketch of the support system on which the cylinder was mounted at each end, allowing it to move only in the vertical direction. The lower beams (6 m long) and the connecting rods were mounted inside ducts to minimise unwanted hydrodynamic damping. The beams are shown with an exaggerated downwards displacement from their equilibrium position.

2. THE EXPERIMENTS

The experiments were carried out in the Delta Flume at Delft Hydraulics, and the full details of the apparatus are described by Chaplin (2000). The flume is 230 m long, 5 m wide and 7 m deep, and was operated with a still water depth of 5·5 m. The waves were generated by a servo-controlled piston-type wavemarker with automatic second-order corrections to eliminate parasitic waves. At the opposite end of the flume, there was a solid concrete beach with a compound slope of maximum gradient 1:6, and wave reflections were in some conditions rather large. However, in processing the results, measurements of damping were related to measurements of the ambient velocity field in the vertical plane close to the cylinder, rather than to the water surface elevation record.

Figure 1 is a sketch of the main elements of the experimental rig, which was constructed beneath the flume carriage. In the experiments described in this paper, the carriage was stationary, and raised on steel blocks to provide a very stiff foundation for the whole apparatus. The test cylinder, suspended elastically at each end at the mid-points of enclosed horizontal 6 m long steel beams, was 0·75 m in diameter and 4·29 m long, and had a smooth painted external surface finish. At its mean position, it was at an elevation of 3·6 m above the floor of the flume, and 1·9 m below the still water surface. Its total mass was 1179 kg, and (with associated hardware) it was neutrally buoyant. A second pair of beams, parallel to the first, was connected to the top of vertical connecting rods attached to each end of the cylinder. The natural frequency of the cylinder support system could be altered by using upper beams of different stiffnesses. Experimental conditions are mentioned in Table 1.

The vertical motion of the cylinder was measured by detecting the curvature of the lower beams by means of strain gauges. The issues of calibrations, endplates, and tare damping (including that due to wavemaking), are discussed in Chaplin (2000). A significant difference in the experiments described here was the use of continuous force excitation, generated by means of a variable speed motor mounted on a cross-beam spanning the flume between the

TABLE 1
Experimental conditions, with natural frequencies measured in air and water

Case (1)	Nat. freq. in air (Hz) (2)	Stiffness (kN/m) (3)	Submerged nat. freq., f_n (Hz) (4)	β (5)	$26{\cdot}24/\sqrt{\beta}$ (6)	Series (7)	Total tare damping, ζ_s (8)
1	3·210	281	1·312	647 000	0·0326	WSE	0·0019
						WSF	0·0019
2	3·442	659	2·020	997 000	0·0263	WSB	0·0079
						WSC	0·0019

mid-points of the two upper beams. The output shaft of the motor was connected by a crank to a vertical rod, which was free to move vertically in linear bearings. By clamping steel discs to the rod, its total oscillating mass could be adjusted in steps up to 25 kg. This out-of-balance system provided a means of applying a vertical harmonic excitation to the cylinder of known frequency (determined by the finely controlled speed of the motor) and amplitude [determined by the amplitude (65 mm) of the motion of the rod relative to the cross-beam, the oscillating mass, and the frequency]. It was used as before to start free decay tests, but in this case also to excite the cylinder in steady-state oscillations. The phase of the excitation was provided by a displacement transducer that measured the motion of the rod relative to the cross-beam.

Particle velocities were measured by an electro-magnetic velocity meter positioned at the elevation of the axis of the cylinder, but 6 m further towards the wavemaker and about 1 m from the tank wall, and two wave gauges measured the instantaneous water surface elevation, one directly above the cylinder, and the other on the same tank cross-section as the velocity meter.

From the same programme of large scale tests, Johanning *et al.* (2001) describe measurements of the damping of oscillations of a vertical surface-piercing cylinder.

3. DISCUSSION OF THE MEASUREMENTS

3.1. MEASUREMENTS OF DAMPING IN FREE DECAY

Measurements were made in regular waves of periods 4 and 8 s. The conditions are shown in Table 2, which include the ratios (in the range 5·25–16·16) between the cylinder natural frequency when oscillating at small amplitudes in still water f_n and the wave frequency f_w. The results of tests in which the oscillation of the cylinder decayed freely in the presence of waves are considered first. Each experiment was started by displacing the cylinder manually, or by exciting it with the motor system for a short time at a frequency close to its natural frequency, and its damping was obtained from the subsequent decaying motion. As an example, one set of results is shown in Figure 2.

A Keulegan Carpenter number was computed for each cycle of the cylinder oscillation, and the resulting sequence $K(n)$ was then fitted [as shown in Figure 2(c)] to the formula,

$$K = R\exp(-2\pi\zeta n) + K_0, \tag{5}$$

where R is a constant, ζ is the damping expressed as a proportion of critical, and K_0 is the mean Keulegan Carpenter number of steady-state oscillations that occurred after the effects of the external excitation had completely died away. The measured damping factor ζ is the

TABLE 2
Wave conditions. The amplitudes of the fundamental frequency components of the horizontal and vertical wave-induced flow are u_1 and w_1; $K_1 = u_1/f_w d$

Case (1)	Series (2)	Wave period (s) (3)	Nominal wave heights (m) (4)	f_n/f_w (5)	u_1 (m/s) (6)	w_1(m/s) (7)	K_1 (8)
1	WSE	4·00	0·1–1·0	5·25	0·07–0·53	0·02–0·40	0·24–2·50
	WSF	8·00	0·1–1·2	10·50	0·10–0·57	0·02–0·29	0·69–5·25
2	WSB	4·00	0·1–1·0	8·08	0·07–0·52	0·02–0·41	0·26–2·55
	WSC	8·00	0·1–1·2	16·16	0·18–0·56	0·04–0·30	0·73–5·31

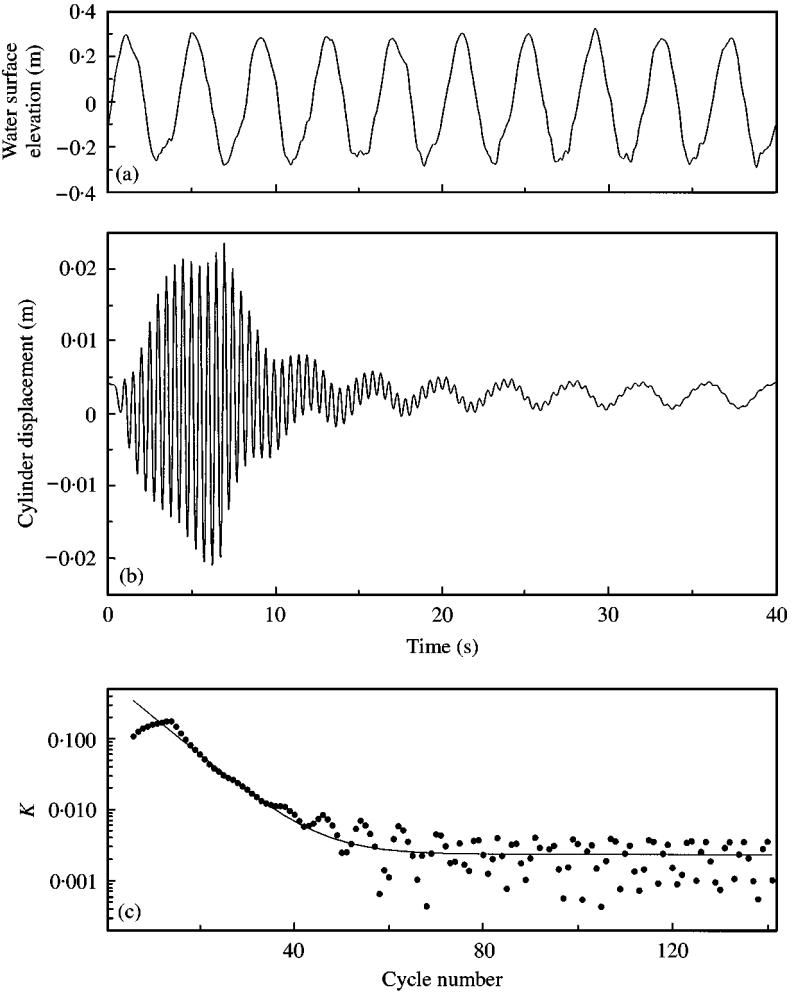

Figure 2. Time series for (a) the water surface elevation above the cylinder, and (b) the vertical response of the cylinder following an initial excitation in test WSB008. In (c) the decaying motion of the cylinder is plotted in the form of the Keulegan Carpenter number of each cycle of oscillation. A line shows the best fit of the form of equation (5).

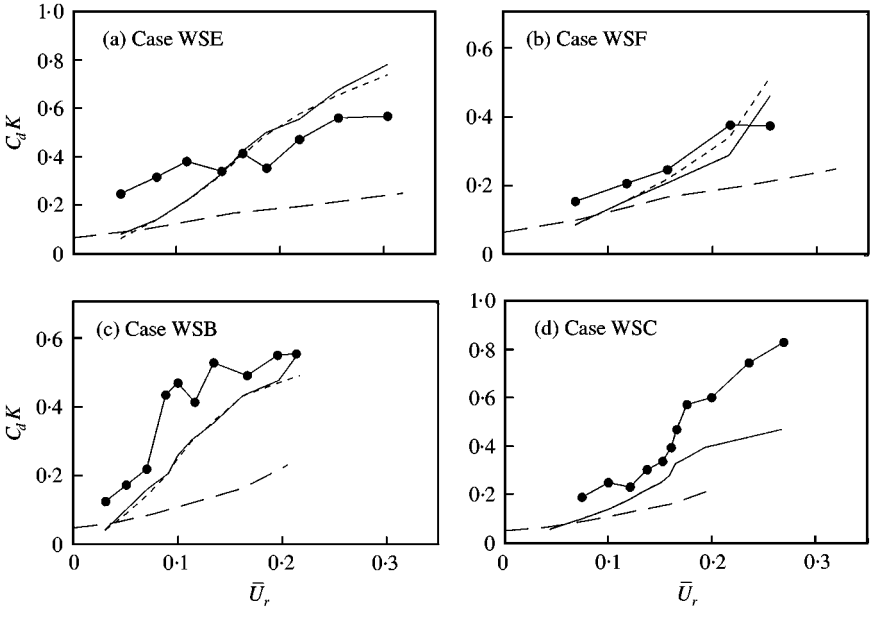

Figure 3. Damping factors C_dK for oscillations in waves, plotted against the mean of the reduced velocity $U_r = |U_x|/fd$. Measurements obtained in free decay tests are shown as points joined with a continuous line. A second continuous line in each case shows the Morison prediction based on equation (4), and a short-dashed line is the approximation of equation (9). Long-dashed lines show the damping measured in very slowly varying horizontal currents at similar values of β (Chaplin 2000).

sum of the hydrodynamic damping ζ_h and the known tare damping ζ_s, and the former is related to the drag coefficient by

$$C_d = \frac{3\pi^3 m\zeta_h}{4MK} \tag{6}$$

(Sumer & Fredsøe 1997, p. 349), where m is the total oscillating mass (in the present case, about 4000 kg including the added mass) and M is the displaced mass of the cylinder (1895 kg).

By this means, we obtained from each test a constant drag coefficient which fitted the observed decay of the motion over a range of Keulegan Carpenter numbers. This range was limited at the upper end by the initial amplitude of the cylinder, and further by the fact that largely owing to transient effects, the amplitudes of the first few oscillations did not match equation (5), (as can be seen in Figure 2). At the lower end, the range was limited by the amplitude of the wave-excited motion of the cylinder, below which the mean hydrodynamic damping is effectively negative. The actual range over which equation (5) could be fitted to the results was typically in the region of $0{\cdot}01 > K > 0{\cdot}005$.

It is convenient as before to present the results in terms of values of C_dK, since for given experimental conditions this product is proportional to ζ_h, and theoretically, in still water it approaches a constant value of $26{\cdot}24\sqrt{\beta}$—the values of which appear in Table 1. In Figure 3, the values of C_dK derived from the measurements are plotted as functions of the reduced velocity U_r computed from the mean value of the absolute horizontal component of the ambient flow $|U_x|$.

Also shown in Figure 3, in each case, is a long-broken line which represents (for the same value of β) the hydrodynamic damping measured previously in the case of a cylinder

oscillating transversely at similar Keulegan Carpenter numbers in very slowly varying current. In waves at a given reduced velocity, the damping is seen to be considerably higher. This may be due to the unsteadiness of the ambient flow, as well as to the fact that, owing to the orbital motion of the waves, it generally has a component in-line with the cylinder motion, in which conditions for damping can be expected to be higher than for the case of oscillations in a purely transverse current.

Continuous lines in each plot in Figure 3 represent numerical predictions of the damping obtained from Morison's equation (4), with $C_{dr} = 1$ and $C_m = 2$. (These values are adopted in all of the simulations below. The added mass coefficients that were computed from the measurements were close to unity in all cases.) The predicted factors $C_{dp}K$ were computed as follows. For a given relative incident flow, which was the measured velocity record $(U_x(t), U_z(t))$ filtered to remove components at frequencies above 1 Hz, and a cylinder motion $V = Kdf\cos 2\pi ft$, defined by a given Keulegan Carpenter number K and frequency f, a time series for the vertical force on the cylinder was computed from (4). The amplitude $F_z^{(1)}$ of the fundamental frequency component of the simulated force within each time slice of duration $1/f$ was expressed as

$$F_z^{(1)} = \frac{8}{3\pi} C_{dp} \frac{1}{2} \rho d(Kdf) \tag{7}$$

[in which the right-hand side is the amplitude of the fundamental frequency component of $C_{dp}(\frac{1}{2}\rho V|V|d)$], in order to provide a sequence of values of $C_{dp}K$, from which the mean was calculated over a large number of waves. This depends on the input Keulegan Carpenter number K, and becomes negative for small K as a consequence of the wave excitation of the cylinder. But once the chosen value of K exceeds that corresponding to the steady-state oscillation of the cylinder K_0, the computed damping factor is initially almost independent of K, and the results shown in Figure 3 refer to this range.

A simple approximation for this simulated damping factor can be obtained for the case when the cylinder frequency is much greater than the wave frequency ($f/f_w \gg 1$), but its velocity is much smaller than that of the wave-induced flow ($V \ll \sqrt{U_x^2 + U_2^2}$). Such a case would be $f/f_w = 10$ and $K/K_w = 0{\cdot}01$, where K_w is a wave Keulegan Carpenter number,

$$K_w = \frac{\overline{\sqrt{U_x^2 + U_z^2\,[1 + U_z^2/(U_x^2 + U_z^2)}}}{f_w d}. \tag{8}$$

Under these conditions, equation (4) reduces to a form that indicates a mean level of damping corresponding to

$$C_{dp}K = \frac{3\pi}{8} C_{dr} K_w \frac{f_w}{f}. \tag{9}$$

This is shown in each case in Figure 3 as a short-dashed line, and as expected matches the corresponding numerical simulation quite well.

Bearing in mind that no attempt has been made to optimise the values of the drag and inertia coefficients, the predictions match the measurements quite closely, and the agreement is much better than might be expected from previous discussion of the relative velocity Morison's equation. Moe & Verley (1980) found this approach to be grossly unconservative in many cases (i.e., it may led to over-predictions of the damping); but in their case and in that of Demirbilek *et al.* (1987), Reynolds numbers were considerably lower, and the relative amplitude of the cylinder motion was considerably greater. Figure 3 shows that in the present conditions Morison's equation leads in many cases to an under-prediction of the

measured damping, but its behaviour is quite similar and indicates that values of C_{dr} not far from unity would lead to reasonably accurate predictions of the damping.

3.2. Frequency and Amplitude of the Cylinder Steady-State Response

It is interesting to examine the relationship between the cylinder frequency and the wave frequency in the steady state, as seen at large times in Figure 2, when the cylinder was oscillating freely in waves after all the effects of the external excitation had died away. The ratios obtained in Table 2 refer to the cylinder natural frequency when oscillating at small amplitudes is still water, but these were generally changed by the presence of waves. Shifts in the frequency of the cylinder can be attributed to the change in added mass, which is to be expected in those conditions, but a notable feature of the measurements was a tendency of the cylinder to become locked on to a multiple wave frequency. This behaviour is well known in the case of a cylinder oscillating transversely in a harmonic rectilinear flow, in conditions where the peak reduced velocity is between 4 and 20 (and vortex shedding forces are dominant in the cross-flow direction), and where the amplitude of the undisturbed fluid motion is many times greater than the cylinder diameter [see, e.g., Sumer & Fredsøe (1997)]. In the present conditions, on the other hand, the reduced velocity was always less than 0·3, and the Keulegan Carpenter number of the wave flow K_w was less than 4 in almost all cases.

To identify when lock-on was occurring, we first computed the fundamental frequency component of the cylinder motion over each cycle of its high-frequency oscillation, and identified the instant at which this filtered displacement record reached a maximum elevation. The corresponding Keulegan Carpenter number was then plotted against the instantaneous elevation of the water surface above the cylinder, as an indication of the phase of the ambient flow. Examples are shown in Figure 4, including sequences of many waves in each of the four cases. A point is plotted for each oscillation of the cylinder, but at intervals of the integer n nearest to the frequency ratio in column 5 of Table 2; the empty symbols are replaced by a solid one.

The close clustering of points in Figure 4(b) indicates that the fundamental component of the cylinder displacement reached a maximum at almost exactly the same five phases in each passing wave, and that the amplitudes of each oscillation in each wave were highly repeatable. In the conditions of Figure 4(a), with smaller waves at the same frequency, the amplitudes of the cylinder motion followed the same changes through each wave, but its phase was uncoupled to that of the ambient flow. The phase of the cylinder motion processed through the wave without apparent interaction. There was also no indication of lock-on at any other value of n.

At higher frequency ratios, both the lock-on and the repeatability of the amplitudes of the cylinder motion through each wave became weaker. In much larger waves and at $n = 8$, Figure 4(c) shows the same behaviour as Figure 4(a), and in Figure 4(d) for $n = 16$ (in more nonlinear waves), the cylinder was at the same phase of its motion at each wave trough, but its displacement at other times was poorly correlated with the ambient flow.

It seems reasonable to associate those observations with vortex shedding, and the apparent fragility of the lock-on mechanism with the fact that here both the Keulegan Carpenter number of the ambient flow, and its reduced velocity, are well outside the ranges normally associated with this process.

Numerical simulations of undisturbed response of the cylinder in waves were carried out, but, since the cylinder was represented as a linear dynamic system, they did not reproduce any lock-on. The simulations used a Newmark integration scheme to compute the cylinder response in the time domain to the loading given at each instant by equation (4), with the filtered measurements of the wave-induced horizontal and vertical velocity components.

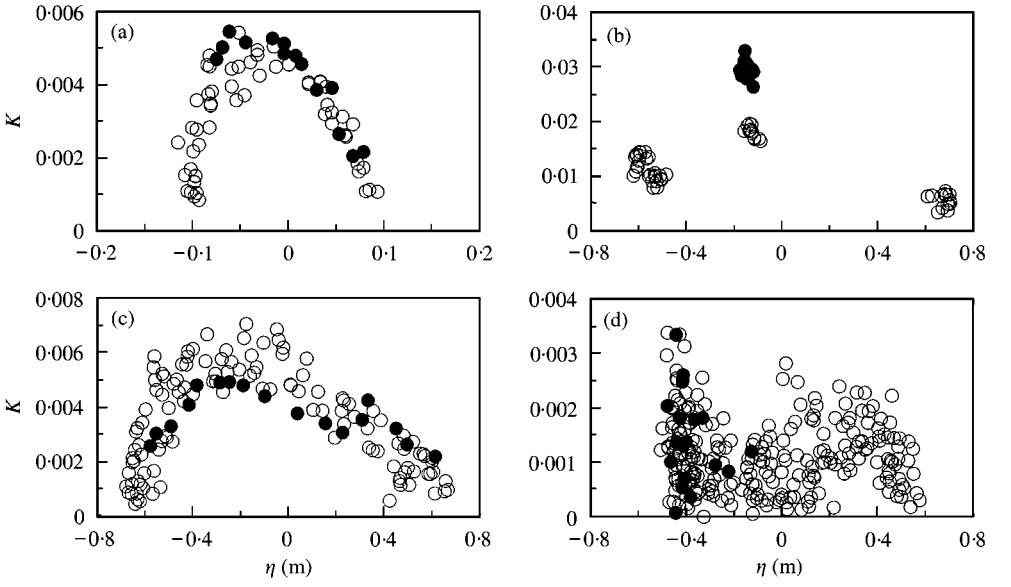

Figure 4. The Keulegan Carpenter number of each oscillation of the cylinder is plotted as a function of the water surface elevation above the cylinder at the instant in the same cycle at which the cylinder reached a maximum vertical displacement. Each nth point is filled, where n is the integer nearest to the ratio of the cylinder natural frequency f_n to the wave frequency f_w (Table 2, column 5). (a) Case WSE, $K_w = 0{\cdot}27$; (b) WSE, $K_w = 3{\cdot}49$; (c) WSB, $K_w = 3{\cdot}50$; (d) WSC, $K_w = 3{\cdot}03$.

The simulated and measured time series for each test were then treated in the same way to provide a Keulegan Carpenter number corresponding to the average amplitude of the cylinder motion at its dominant frequency in the steady state over many waves. The results are compared in Figure 5, and again confirm that in the present conditions, the relative velocity Morison's equation provides reasonable predictions with $C_{dr} = 1$, though there is a tendency for it to over-predict the response in larger waves.

3.3. Response to Steady-State Excitation

In steady-state experiments with continuous external harmonic excitation, the frequency of the excitation system was set similar to the cylinder natural frequency observed in small amplitude oscillations in still water, and the amplitude of the force was set in turn to different values by changing the mass attached to the vertically oscillating rod. By this means, it was possible to compare hydrodynamic damping under steady-state conditions with that observed during a decaying motion.

From the usual theory for a single-degree-of-freedom system, a knowledge of forcing (of amplitude F and frequency ω), the system stiffness k, and the response (of amplitude a at a phase lag ϕ) is in principle sufficient to provide both the oscillating mass m and the damping c (i.e., force per unit velocity) of the system. In the present case, both must be considered unknown. The theoretical results are

$$m = \frac{k}{\omega^2}\left(1 - \frac{\cos\phi}{\alpha}\right), \quad c = \frac{F\sin\phi}{\omega a}. \tag{10}$$

In a lightly damped system, the damping has very little effect on the response except very near resonance, where the frequency ratio $\tau = \omega\sqrt{m/k} \approx 1$. Elsewhere, very small errors in

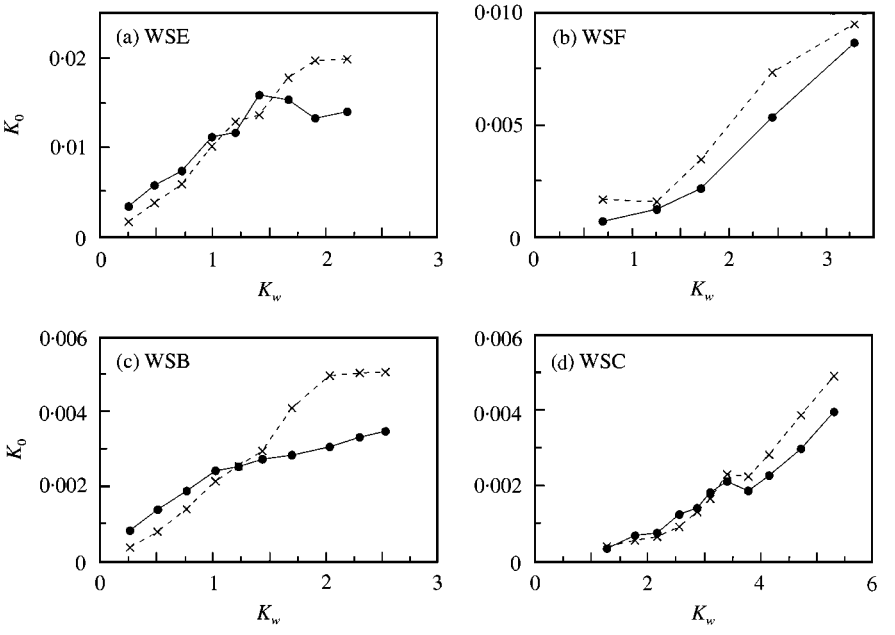

Figure 5. Mean measured and computed Keulegan Carpenter numbers of the cylinder's undisturbed high frequency response in waves as a function of the wave Keulegan Carpenter number defined in equation (8). Measurements are shown with a continuous line, and predictions with a broken line: (a) case WSE; (b) WSF; (c) WSB; (d) WSC.

the measurements of the phase lag ϕ produce much larger errors in the derived values of c. (Uncertainties in all other parameters have proportionately much less impact on the results.) Using data that represent the conditions of the present tests ($m = 4000$ kg, $k = 4 \times 10^5$ N/m), the error in the computed damping factor $\zeta = c/2\sqrt{mk}$ resulting from an error of 1 degree in ϕ in numerically found to be about

$$\frac{\Delta\zeta}{\zeta} = 0{\cdot}017\,\frac{|\tau - 1|}{\zeta} \tag{11}$$

from equations (10). This was large enough to render the method unusable in the still water tests described in Chaplin (2000) where $\zeta \sim 0{\cdot}001$, and very noisy in the present high-frequency cases WSB and WSC. But in the presence of waves, and at appreciable amplitudes of oscillation, the damping in the present experiments was often an order of magnitude greater, and consistent results for ζ were obtained in the low-frequency case WSE, with τ at about 0·988.

The results obtained from equation (10) for the damping were indistinguishable from those computed directly by equating the measured and predicted mean power loss, from which

$$c = \frac{\int Fv\,\mathrm{d}t}{\int v^2\,\mathrm{d}t}, \tag{12}$$

where F is the instantaneous excitation force, and V the velocity of the cylinder, and the integration is taken over a large number of cycles.

Figure 6 compares the damping factor obtained in steady-state oscillations at Keulegan Carpenter numbers of about 0·06 with those found in the free decay tests at similar

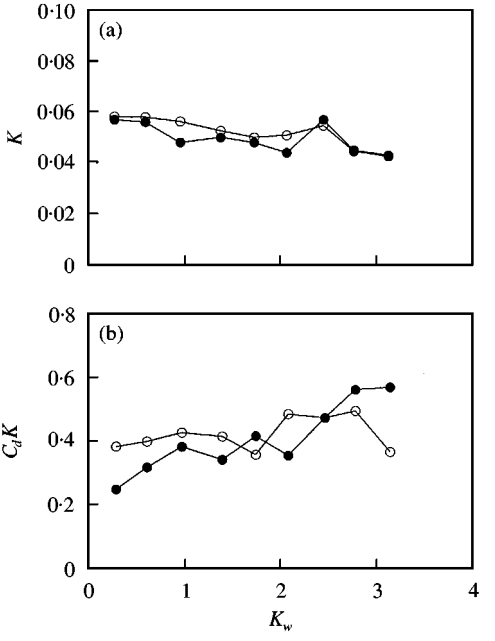

Figure 6. Comparison between results of measurements of steady-state oscillation (●) and decaying oscillations (○) in series WSE. In (a) the Keulegan Carpenter numbers of the cylinder's high-frequency oscillations generated with 10 kg on the force exciter are compared with the maximum Keulegan Carpenter number observed in free decay tests at the same wave amplitude. The corresponding damping factors are shown in (b).

amplitudes of oscillation. There is a reasonable measure of agreement between the two sets of results.

4. CONCLUSIONS

Measurements have been made of the hydrodynamic damping of a circular cylinder oscillating vertically beneath regular progressive waves (whose crests are parallel to the cylinder axis) at values of the Stokes parameter β of 647 000 and 947 000. The ratio of the cylinder frequency to the wave frequency was between 5·15 and 16·16, and attention was focused on very small amplitudes of oscillation with Keulegan Carpenter numbers between 0·01 and 0·1.

In view of the conclusions of previous investigations mentioned above, a notable outcome of this work is that measurements of damping were found to be in quite good agreement with the implications of the vector form of the relative velocity Morison equation. No attempts were made to compute optimal drag and inertia coefficients, but comparisons made with constant values $C_d = 1$, $C_m = 2$, were for most purposes in adequate agreement with the data obtained either in free decay tests or in steady-state oscillations. Important differences with respect to previous studies (Maull & Milliner 1979; Moe & Verley 1980; Demirbilek *et al.* 1987; Chaplin & Subbiah 1998) are that, in our case, the amplitudes of motion were considerably smaller, and Reynolds numbers were higher by almost an order of magnitude or, in some cases, much more. There is still a considerable gap between the Reynolds numbers of the present tests and those of applications offshore, and in particular it seems unlikely that we have reached post-critical flow in conditions where the Reynolds number of the wave-induced flow $U_r\beta$ is only of order 10^5. Only measurements at

still larger scale can answer the question of what scale effects remain, and whether this form of Morison's equation is still appropriate at Reynolds numbers two orders of magnitude higher.

The response of the cylinder at its natural frequency to wave-induced excitation was also quite well predicted by Morison's equation. In some cases at wave Keulegan Carpenter numbers K_w as low as 3·5 there was clear evidence of lock-on, during which the displacement of the cylinder became locked to the phase of the wave at an integer frequency ratio. This seems not to have had much influence on the amplitude of its motion.

ACKNOWLEDGEMENTS

Access to the Delta Flume was provided through the TMR programme of the European Commission. Funding for other elements of this work was provided by the EPSRC (Contract GR/M10113). The assistance of Teit Schønberg in some final calibration tests is gratefully acknowledged.

REFERENCES

CHAPLIN, J. R. 2000 Hydrodynamic damping of a cylinder at $\beta \approx 10^6$. *Journal of Fluids & Structures* **14,** 1101–1117.

CHAPLIN, J. R. & SUBBIAH, K. 1998 Hydrodynamic damping of a cylinder in still water and in a transverse current. *Applied Ocean Research* **20,** 251–259.

DEMIRBILEK, Z., MOE, G. & YTTERVOLL, P. O. 1987 Morison's formula: relative velocity versus independent flow fields formulation for a case representing fluid damping. *Proceedings of the Sixth OMAE Conference* Vol. 2 pp. 25–31.

HALL, P. 1984 On the stability of unsteady boundary layer on a cylinder oscillating transversely in a viscous fluid. *Journal of Fluid Mechanics* **146,** 337–367.

JOHANNING, L., BEARMAN, P. W. & GRAHAM, J. M. R. 2001 Hydrodynamic damping of a large scale surface piercing circular cylinder in planar oscillatory motion. *Journal of Fluids & Structures* **15,** 891–908.

MAULL, D. J. & MILLINER, M. G. 1979 The forces on a circular cylinder having a complex periodic motion. In *Mechanics of Wave-induced Forces on Cylinders* (ed. T. L. Shaw) London: Pitman, pp. 490–502.

MAULL, D. J. & NORMAN, S. G. 1979 A horizontal circular cylinder under waves. In *Mechanics of Wave-induced Forces on Cylinders* (ed. T. L. Shaw) London: Pitman, pp. 359–378.

MOE, G. & VERLEY, R. L. P. 1980 Hydrodynamic damping of offshore structures in waves and currents. OTC paper 3798, *Proceedings of the OTC*, pp. 37–44.

STOKES, G. G. 1851 On the effect of the internal friction of fluids on the motion of pendulums. *Transactions of the Cambridge Philosophical Society* **9,** 8–106.

SUMER, B. M. & FREDSØE, 1997 *Hydrodynamics around Cylindrical Structures.* Singapore: World Scientific.

WANG, C.-Y. 1968 On high frequency oscillating viscous flows. *Journal of Fluid Mechanics* **32,** 55–68.

YAN, B. 2000 Unsteady viscous flow about a submerged circular cylinder with a steady current. *Fluid Dynamics Research* **26,** 69–94.